AD-A187 005 EVALUATION OF A TEMPERATURE REMOTE SENSING TECHNIQUE (U) JOHNS HOPKINS UNIV LAUREL MD APPLIED PHYSICS LAB S A GEARHART ET AL. JUL 87 JHU/APL/TG-1365 1/1

UNCLASSIFIED N00039-87-C-5301 F/G 14/2 NL

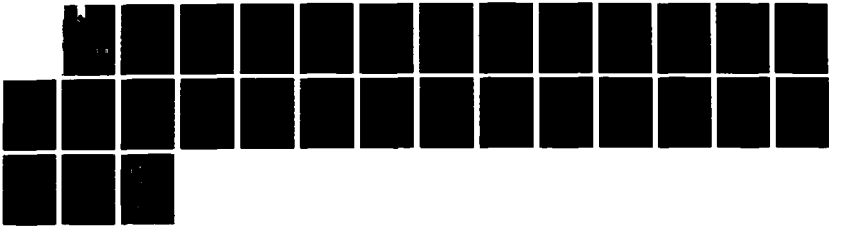

JHU/APL
TG 1365
JULY 1987

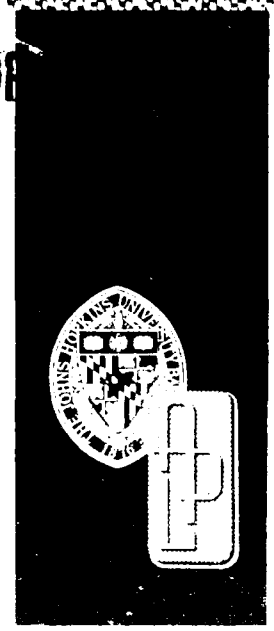

Technical Memorandum

EVALUATION OF A TEMPERATURE REMOTE SENSING TECHNIQUE

S. A. GEARHART and M. E. THOMAS

UNCLASSIFIED

SECURITY CLASSIFICATION OF THIS PAGE

A187 215

REPORT DOCUMENTATION PAGE

1a REPORT SECURITY CLASSIFICATION UNCLASSIFIED	1b RESTRICTIVE MARKINGS
2a SECURITY CLASSIFICATION AUTHORITY	3 DISTRIBUTION/AVAILABILITY OF REPORT Approved for public release; distribution unlimited.
2b DECLASSIFICATION/DOWNGRADING SCHEDULE	
4 PERFORMING ORGANIZATION NUMBER(S) JHU/APL TG 1365	5 MONITORING ORGANIZATION REPORT NUMBER(S) JHU/APL TG 1365
6a NAME OF PERFORMING ORGANIZATION The Johns Hopkins University Applied Physics Laboratory 6b OFFICE SYMBOL (If Applicable) TIR	7a NAME OF MONITORING ORGANIZATION NAVPRO, Laurel, Maryland
6c ADDRESS (City, State, and ZIP Code) Johns Hopkins Road Laurel, Maryland 20707	7b ADDRESS (City, State, and ZIP Code) Johns Hopkins Road Laurel, Maryland 20707
8a NAME OF FUNDING/SPONSORING ORGANIZATION JHU APL Independent Research and Development Program 8b OFFICE SYMBOL (If Applicable) FIF	9 PROCUREMENT INSTRUMENT IDENTIFICATION NUMBER N00039-87-C-5301
8c ADDRESS (City, State, and ZIP Code) Johns Hopkins Road Laurel, Maryland 20707	10 SOURCE OF FUNDING NUMBERS PROGRAM ELEMENT NO / PROJECT NO / TASK NO: X8G5 / WORK UNIT ACCESSION NO

11 TITLE (Include Security Classification)

Evaluation of a Temperature Remote Sensing Technique (U).

12 PERSONAL AUTHOR(S)

Gearhart, S. A. and Thomas, M. E.

13a TYPE OF REPORT	13b TIME COVERED	14 DATE OF REPORT (Year, Month, Day)	15 PAGE COUNT
Technical Memorandum	FROM TO	1987, July	30

16 SUPPLEMENTARY NOTATION

17 COSATI CODES			18 SUBJECT TERMS
FIELD	GROUP	SUB-GROUP	Combustion diagnostics; Laser absorption technique; Laser remote sensing; Noninvasive instrumentation; Temperature sensing

19 ABSTRACT (Continue on reverse if necessary and identify by block number)

A noninvasive technique for measuring temperature in hot gases is evaluated as an alternative to conventional mechanical probing techniques. The technique uses a diode laser spectrometer to measure the line-center absorption coefficient ratio of two absorption lines that originate from different vibrational energy levels of the same absorbing species. The temperature is calculated without knowledge of the pressure, absorber concentration, or optical length. A previous study demonstrated temperature measurements at about 2000 K at atmospheric pressure. The results of this evaluation suggest that the technique is also applicable for temperatures as low as 400 K and at pressures well below 1 atm.

20 DISTRIBUTION/AVAILABILITY OF ABSTRACT	21 ABSTRACT SECURITY CLASSIFICATION
☒ UNCLASSIFIED/UNLIMITED ☐ SAME AS RPT ☐ DTIC USERS	UNCLASSIFIED
22a NAME OF RESPONSIBLE INDIVIDUAL NAVPRO Security Officer	22b TELEPHONE (Include Area Code) (301) 953-5403 / 22c OFFICE SYMBOL NAVPRO SE

DD FORM 1473, 84 MAR

83 APR edition may be used until exhausted
All other editions are obsolete

SECURITY CLASSIFICATION OF THIS PAGE

UNCLASSIFIED

JHU/APL/
TG-1365
JULY 1987

Technical Memorandum

EVALUATION OF A TEMPERATURE REMOTE SENSING TECHNIQUE

S. A. GEARHART and M. E. THOMAS

THE JOHNS HOPKINS UNIVERSITY ■ APPLIED PHYSICS LABORATORY
Johns Hopkins Road, Laurel, Maryland 20707
Operating under Contract N00039-87-C-5301 with the Department of the Navy

ABSTRACT

A noninvasive technique for measuring temperature in hot gases is evaluated as an alternative to conventional mechanical probing techniques. The technique uses a diode laser spectrometer to measure the line-center absorption coefficient ratio of two absorption lines that originate from different vibrational energy levels of the same absorbing species. The temperature is calculated without knowledge of the pressure, absorber concentration, or optical path length. A previous study demonstrated temperature measurements at about 2000 K at atmospheric pressure. The results of this evaluation suggest that the technique is also applicable for temperatures as low as 400 K and at pressures well below 1 atm.

CONTENTS

List of Figures 6

1.0 Introduction 7

2.0 Concept 8
2.1 An Overview of Absorption Theory 8
2.2 The Temperature Dependence of the Line-Center Absorption Coefficient Ratio of Two Absorption Lines 10
2.3 Absorption Line Selection 11

3.0 Experimental Setup 12
3.1 Test Setup 12
3.2 Apparatus 13
3.2.1 The Diode Laser System 13
3.2.2 The Test Cell 14

4.0 Measurements 15
4.1 Measurement Procedures 16
4.2 Results 17
4.2.1 Results of Measurements in the Doppler Regime 17
4.2.2 Results of Measurements in the Collision Regime 18
4.3 Error Analysis 20
4.3.1 Transmittance Measurement Errors 20
4.3.2 Temperature Uncertainty 21

5.0 Conclusions 23

Appendix A: The AFGL Absorption Line Compilation 24

Appendix B: The Spectra of Diatomic Molecules 25

References 27

FIGURES

1. The temperature remote sensing concept....8
2. Laser absorption in a gas....8
3. The ratio of collision linewidth to Doppler linewidth for the $C^{12}O^{16}$ 1-0 P(1) absorption line....10
4. The effect of increasing temperature on energy state populations and absorption line transmittance profiles....10
5. Absorption spectrum of CO measured using a Fourier transform spectrometer and test cell....12
6. Experimental setup and apparatus....13
7. Diode laser tuning characteristics....14
8. The test cell and vacuum enclosure configuration....15
9. Absorption line transmittance measurement....16
10. Temperature measurements in the Doppler regime....17
11. Temperature measurements in the Doppler pressure regime....17
12. Transmittance profiles of three Doppler-broadened CO absorption lines....18
13. Temperature measurements in the Doppler pressure regime. (The modified STP line strength of $C^{12}O^{16}$ 1-0 P(1) was used.)....18
14. Temperature measurements in both the Doppler and collision regimes....19
15. Transmittance profiles of two collision-broadened CO absorption lines....19
16. Temperature measurements in both Doppler and collision regimes. (The modified STP line strength of $C^{12}O^{16}$ 1-0 P(1) was used.)....19
17. Theoretical transmittance profiles of two collision-broadened CO absorption lines at various pressures. Temperature = 773 K....20
18. Theoretical transmittance profiles of two collision-broadened CO absorption lines at various pressures. Temperature = 1273 K....20
19. Etalon-like degradations in transmittance spectra....21
20. Scan-to-scan repeatability of the background transmittance level....21
21. Temperature uncertainty calculations for the matched line pair in the Doppler-broadened regime....22
22. Temperature uncertainty calculations for the matched line pair in the collision-broadened regime....22
23. Temperature uncertainty calculations for the mixed line pair in the Doppler-broadened regime....22
B-1. Energy levels and spectrum of a diatomic molecule....26

THE JOHNS HOPKINS UNIVERSITY
APPLIED PHYSICS LABORATORY
LAUREL, MARYLAND

1.0 INTRODUCTION

Astrophysicists have long relied on measurements of electromagnetic spectra to determine remotely many properties of celestial bodies, such as their temperature, pressure, and chemical composition. With recent advances in optics and quantum electronics, similar spectroscopic techniques are now being employed for other applications that require a remote, noninvasive measurement. For example, Reid et al.[1] used a tunable diode laser spectroscopic technique to identify and monitor air pollutants remotely. A similar technique has been proposed by Cassidy et al.[2] to measure the pressure of trace gases in the atmosphere. In addition, Raman spectroscopy and coherent Raman anti-Stokes spectroscopy (CARS) techniques have been investigated to measure temperature and molecular concentration for flow and combustion diagnostics.[3,4]

This study examines a spectroscopic remote sensing technique that was first proposed by Wang[5] to measure temperatures of hot gases noninvasively. The technique uses a tunable laser to probe the gas and measure the line-center transmittances of two absorption lines that originate from different vibration-rotation transitions of the same molecular species. The ratio of the line-center absorption coefficients, calculated from the measured transmittances, determines the temperature of the gas. Hanson et al.[6] demonstrated this technique, using a tunable diode laser and two carbon monoxide absorption lines to measure temperatures in a flame. The temperature uncertainty at 2100 K is quoted to be better than $\pm 2\%$.

The dual-line ratio technique has two major advantages over the Raman spectroscopic and CARS techniques mentioned above. First, a relatively strong laser signal is measured as opposed to conventional Raman spectroscopy, which requires the measurement of relatively weak fluorescence. Consequently, the detection signal-to-noise ratio is significantly greater. Although the signal-to-noise ratio in the CARS technique is typically good, high powered tunable lasers are required. Furthermore, the decoupling of temperature from absorber concentration in the measured CARS signal is difficult and requires extensive calibration and data processing. By comparison, the dual-line ratio technique uses low power, relatively low cost diode lasers, and requires minimal knowledge of other gas parameters (i.e., pressure, path length, and absorber concentration).

The disadvantage of the dual-line ratio technique is that it does not measure temperature at a point, but along a homogeneous path. However, Wang[5] has proposed extending the technique to measure a cross section of gas by taking many line measurements along different paths and extracting point data via computer-aided tomographic techniques. With future advances in diode laser technology, for example the development of single-mode lasers that do not require cooling from a closed-cycle cryogenic refrigerator, a diode laser system may soon be compact enough to make temperature tomography possible for many practical applications. Indeed, such a system may be significantly simpler to implement than the rival techniques mentioned above.

The intent of this study is to examine both analytically and experimentally the dual-line ratio technique and identify the parameters that are critical in practical applications. Since previous studies have demonstrated the basic feasiblity for high temperature measurements (at about 2000 K),[6] the applicability for temperature measurements below 1000 K is emphasized. Various total pressure regimes are also examined, as well as absorption line selection criteria. One potential use for the technique is to monitor temperature in a supersonic aerodynamic test facility such as the one at The Johns Hopkins University Applied Physics Laboratory.

---

[1] J. Reid, J. Shewchun, B. K. Garside, and E. A. Ballik, "Detecting Pollutants in the Atmosphere," *Appl. Opt.* **17** (Jan 1978).

[2] D. T. Cassidy and J. Reid, "Atmospheric Monitoring of Trace Gases," *Appl. Opt.* **21** (Apr 1982).

[3] M. D. Levenson, "Coherent Raman Spectroscopy," *Phys. Today* (May 1977).

[4] T. T. Lee, R. Turner, and R. C. Benson, "Optical Measurements for Ramjet Engine Development," *Johns Hopkins APL Tech. Dig.* (Jul.–Sep. 1983).

[5] T. Y. Wang, "Laser Absorption Methods for Simultaneous Determination of Temperature and Species Concentration Through a Cross Section of Radiating Flow," *Appl. Opt.* **15** (Mar 1976).

[6] R. K. Hanson and P. K. Falcone, "Temperature Measurement Technique for High Temperature Gases Using a Tunable Diode Laser," *Appl. Opt.* **17** (Aug 1978).

2.0 CONCEPT

Figure 1 is a block diagram of the remote sensing concept. The beam from a tunable laser is passed through the gaseous test medium to a radiation detector. The frequency of the beam is tuned through two absorption lines of the gas. The temperature of the gas is then determined from the measured transmittance profiles. The equations for determining the temperature from transmittance measurements are developed below. The criteria for selecting the absorption lines are also presented.

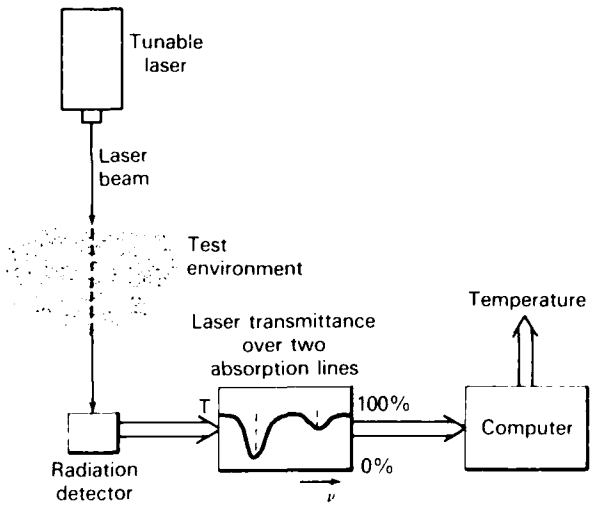

Figure 1 The temperature remote sensing concept.

2.1 AN OVERVIEW OF ABSORPTION THEORY

When molecules are irradiated with a continuous spectrum of photons, the transmitted spectrum contains dark lines that correspond to absorption at discrete frequencies. The frequency at which an "absorption line" appears is proportional to the energy required to excite each absorbing molecule from a lower to higher energy configuration. The distribution of absorption lines is characteristic of the structure of the absorbing molecule.

Consider a laser beam of intensity I_0 passing through a gaseous medium as shown in Fig. 2. If the energy of the laser beam (i.e., the frequency) is approximately equal to the energy difference between two quantum energy levels of the gas molecules and if the

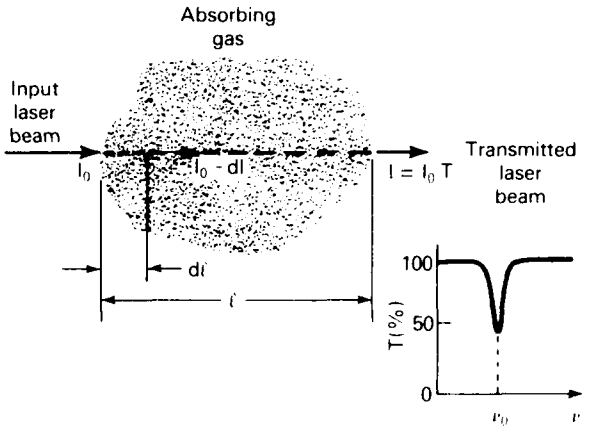

Figure 2 Laser absorption in a gas.

transition from one energy level to the other is allowed (given quantum mechanical constraints), then the laser energy is absorbed, causing a sharp reduction in transmittance. The change in intensity of the beam after passing an infinitesimal distance into the gas is $-dI$, where

$$dI(\nu) = -k(\nu)d\ell \,. \tag{1}$$

Equation 1 is Lambert's law for the absorption of radiation. Solving the differential equation gives the transmittance of the beam through a thickness, or path length, ℓ; thus,

$$T(\nu) = \frac{I(\nu)}{I_0} = e^{-k(\nu)\ell} \,. \tag{2}$$

The transmittance of the laser as a function of frequency defines the shape of the absorption line. The absorption coefficient, k, can be expressed as the product of two terms: S, the linestrength, and $g(\nu,\nu_0)$, the lineshape function

$$k(\nu) = Sg(\nu,\nu_0) \tag{3}$$

where ν_0 is the line-center wavenumber.

The linestrength determines the intensity of the absorption line per unit path length. The linestrength depends on the difference between the number of molecules that are initially residing in each of the two energy states of the corresponding energy transition, as determined by the temperature and pressure of the absorb-

ing species and the probability that the transition will occur. The derivation of the linestrength is lengthy and not integral to this discussion; therefore, one commonly used expression is simply stated below:

$$S = S_0 \frac{T_0}{T} \frac{P_a}{P_{a_0}} \frac{Q_{E_0} Q_{V_0} Q_{R_0}}{Q_E Q_V Q_R} \times \exp\left[E_\ell \left(\frac{T - T_0}{k_B T T_0}\right)\right] \times \frac{1 - \exp(-hc\nu_0/k_B T)}{1 - \exp(-hc\nu_0/k_B T_0)} , \quad (4)$$

where

T	is the temperature,
P_a	is the partial pressure of the absorbing species,
E_ℓ	is the lower energy level of the transition,
Q_E, Q_V, and Q_R	are the electronic, vibration, and rotation partition functions, respectively, and
k_B, h, and c	are Boltzmann's constant, Planck's constant, and the speed of light, respectively.

The subscript "0" denotes values at a standard temperature and pressure (STP) of 296 K and 1 atm, respectively. Equation 4 expresses the linestrength as the departure from the linestrength value at STP.

The STP parameters that are relevant to this discussion, the linestrength, S, the energy of the lower level of the corresponding transition, E_ℓ, and the line-center wavenumber, ν_0, are obtained from the absorption line parameter listing prepared by the Air Force Geophysics Laboratory (AFGL) for the primary atmospheric species.[7] A computer program that reads the AFGL data tape is provided in Appendix A. Examples of the output are included.

The lineshape function characterizes the frequency spread of the absorption line. It is normalized such that

$$\int_{-\infty}^{+\infty} g(\nu,\nu_0)\, d\nu = 1 . \quad (5)$$

[7] R. A. McClatchey, *AFCRL Atmospheric Absorption Line Parameters Compilation*, distributed by National Technical Information Service (Jan 1973).

The lineshape function can be easily understood from a classical viewpoint by treating each absorbing molecule as an electric dipole that is excited and set into motion by the applied electromagnetic field (i.e., the laser). Using a linear systems analogy, the lineshape function then represents the frequency response of each dipole or more precisely the response of the polarization field produced by the summed fields of all the dipoles, to the applied field. This is directly analogous to the response of a damped spring-mass system to an external driving force. By evaluating the classical equations of motion for a large number of oscillating dipoles, it can be easily shown that the width of the frequency response is related to the decay rate of the resultant polarization field.

In general, at pressures above approximately 0.2 atm, the decay rate of the resultant polarization field, and hence the shape of the lineshape function, is determined by the rate of molecular collisions. This is collision broadening. The collision lineshape is a Lorentzian function given by

$$g_C(\nu,\nu_0) = \frac{2}{\pi\Delta\nu_C} \Big/ \left[1 + \left(\frac{2(\nu - \nu_0)}{\Delta\nu_C}\right)^2\right] . \quad (6)$$

$\Delta\nu_C$, the collision linewidth (the fullwidth at half maximum (FWHM)), is

$$\Delta\nu_C = 2\alpha_0 P_{tot} (T_0/T)^{1/2} , \quad (7)$$

where α_0, the STP FWHM, is obtained from the AFGL compilation. Note that the use of Eq. 7 is restricted to gas mixtures having molecular composition similar to that of the atmosphere. (α_0 can be considered the broadening coefficient for an air mixture.)

At pressures below about 0.02 atm, where atomic collisions are infrequent, the Doppler effect determines the width of the absorption line. Doppler broadening occurs when radiation at an arbitrary frequency is Doppler shifted to the line-center frequency (i.e., the resonant frequency in the moving reference frame of the molecule). Subsequently, because of the velocity distribution of the molecules in the gas, a range of incident frequencies can be absorbed. The Doppler lineshape is a Gaussian function given by

$$g_D(\nu,\nu_0) = \sqrt{\frac{ln(2)}{\pi}}\ \frac{2}{\Delta\nu_D} \times \exp(-ln(2)[2(\nu - \nu_0)/\Delta\nu_0]^2) . \quad (8)$$

The Doppler linewidth (FWHM) is given by

$$\Delta\nu_D = 2\nu_0 \left(\frac{2k_B T\, ln(2)}{Mc^2}\right)^{1/2}, \quad (9)$$

where M is the mass of the absorbing molecule.

At pressures from about 0.02 to 0.2 atm (for temperatures between 500 and 1000 K), both molecular collisions and the Doppler effect contribute to the absorption lineshape. This is the Voigt regime. The Voigt lineshape is expressed as a convolution of the collision and Doppler lineshapes,

$$g_V(\nu,\nu_0) = \int_{-\infty}^{\infty} g_D(\nu')\, g_C(\nu_0 - \nu')\, d\nu' . \quad (10)$$

Figure 3 shows plots of $\Delta\nu_C/\Delta\nu_D$ versus temperature for air-broadened carbon monoxide at a number of pressures. The calculations were performed using Eqs. 7 and 9. The three pressure regimes are marked on the figure.

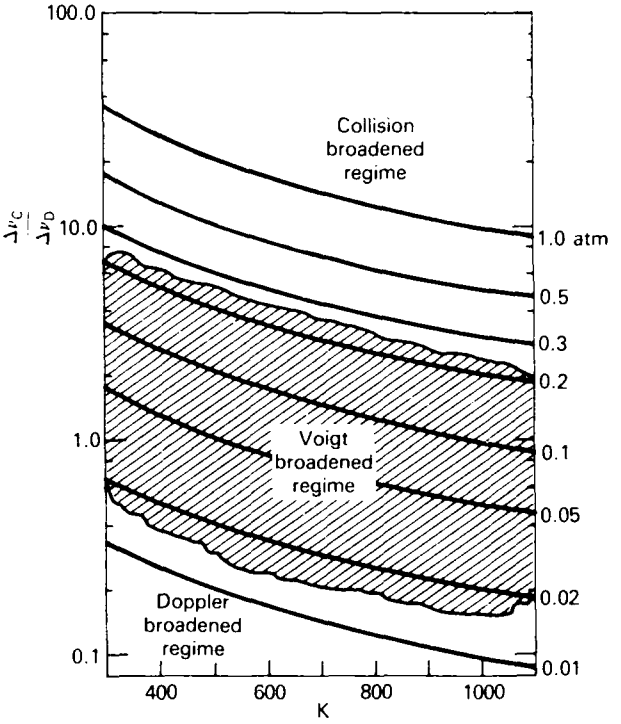

Figure 3 The ratio of collision linewidth to Doppler linewidth for the $C^{12}O^{16}$ 1-0 P(1) absorption line.

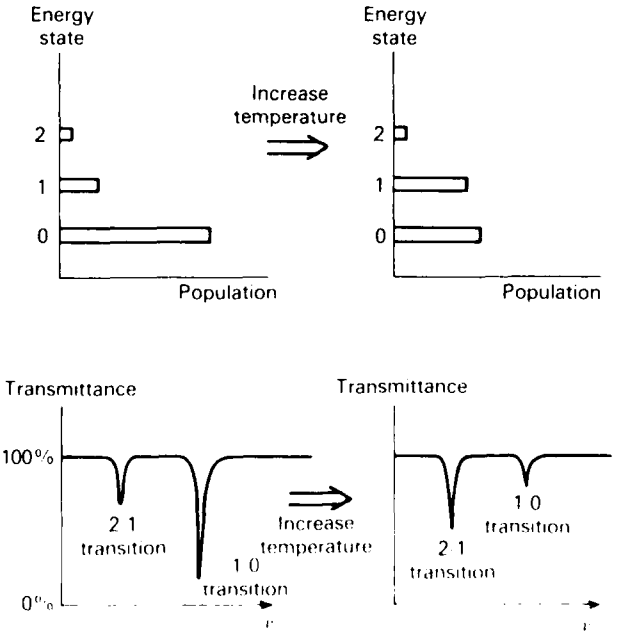

Figure 4 The effect of increasing temperature on energy state populations and absorption line transmittance profiles.

2.2 THE TEMPERATURE DEPENDENCE OF THE LINE-CENTER ABSORPTION COEFFICIENT RATIO OF TWO ABSORPTION LINES

Consider two absorption lines of the same species that are nearly coincident in frequency, and originate from transitions between energy states 0 and 1 and states 1 and 2, respectively, as shown in Fig. 4. As temperature increases, molecules in state 0 are thermally excited to state 1. Because of the decrease in population difference between states 0 and 1, the linestrength of the corresponding absorption line decreases. Conversely, the increase in state 1 population increases the population difference between state 1 and 2, resulting in an increase in the linestrength of the corresponding absorption line. It is the relative behavior of these two absorption lines, as predicted by Maxwell-Boltzmann statistics, that is exploited for the temperature sensing technique examined in this study. This behavior is quantified below. Using Eq. 2, the transmittance ratio of the two lines at their respective line-centers is

$$\frac{T_1(\nu_{01})}{T_2(\nu_{02})} = \frac{\exp[-k_1(\nu_{01})l]}{\exp[-k_2(\nu_{02})l]} . \quad (11)$$

Taking the natural logarithms of the numerator and the denominator gives the absorption coefficient ratio:

$$\frac{ln\ T_1(\nu_{01})}{ln\ T_2(\nu_{02})} = \frac{k_1}{k_2} = \frac{S_1\ g_1(\nu,\nu_{01})}{S_2\ g_2(\nu,\nu_{02})} . \quad (12)$$

Using Eq. 4, this becomes

$$\frac{ln\ T_1(\nu_{01})}{ln\ T_2(\nu_{02})} = \left(\frac{S_{01}}{S_{02}}\right) \times \exp\left[(E_{l1} - E_{l2})\left(\frac{T - T_0}{k_B\ T_0 T}\right)\right] \times \frac{g_1(\nu_{01})}{g_2(\nu_{02})} \quad (13)$$

where the ratio of the factors

$$\frac{\left(\frac{1 - \exp(-hc\nu_{01}/k_B T)}{1 - \exp(-hc\nu_{01}/k_B T_0)}\right)}{\left(\frac{1 - \exp(-hc\nu_{02}/k_B T)}{1 - \exp(-hc\nu_{02}/k_B T_0)}\right)} \approx 1$$

since $\nu_{01} \approx \nu_{02}$. Solving for the temperature and using Eqs. 6 through 9 yields

collision regime

$$T = \frac{T_0}{1 - \frac{k_B T_0}{E_{l1} - E_{l2}} ln\left(\frac{ln(T_1)\ \alpha_{01}\ S_{02}}{ln(T_2)\ \alpha_{02}\ S_{01}}\right)} \quad (14)$$

for pressures in the collision broadened regime, and since $\Delta\nu_{D1} \approx \Delta\nu_{D2}$,

Doppler regime

$$T = \frac{T_0}{1 - \frac{k_B T_0}{E_{l1} - E_{l2}} ln\left(\frac{ln(T_1)\ S_{02}}{ln(T_2)\ S_{01}}\right)} \quad (15)$$

for pressures in the Doppler broadened regime. Equations 14 and 15 indicate that only the line-center transmittances of the two absorption lines need to be measured to determine the temperature of the gas.

At pressures in the Voigt regime, the ratio of the lineshape functions in Eq. 12 will not reduce to a simple expression. To determine the temperature, the natural logarithms of the transmittance profiles (i.e., the absorption profiles) must be integrated, respectively, and ratioed to yield the linestrength ratio, which can then be used in Eq. 15. Because the procedure is somewhat more complicated, this study considers only pressures in the collision and Doppler broadened regimes.

2.3 ABSORPTION LINE SELECTION

For the dual-line ratio technique to be useful in a variety of applications, a number of candidate absorption line pairs must be available. This requirement is satisfied in the infrared (IR) region of the electromagnetic spectrum, where there is a multitude of vibration-rotation absorption lines of various species. The regions from 3 to 5 μm and from 8 to 12 μm are of particular interest because the effects of water vapor absorption is small for short path lengths. The general requirements for selecting absorption lines are:

1. The lines must correspond to different vibrational energy transitions of the same absorbing species,
2. The separation between the lines should be small enough to be scanned with a single frequency sweep of the laser,
3. The separation between the lines should be large enough to preclude significant overlap, and
4. The transmittances of the absorption lines should vary between 10 and 90% over the temperature range of interest.

A number of these requirements are elaborated below.

The maximum absorption line spacing is limited by the continuous tuning capability of the laser. For a tunable IR diode laser, absorption line separations must be about 1 cm^{-1} or less.

The minimum spacing that can be tolerated before the lines overlap significantly is largely dependent on the test environment. For example, at pressures in the collision regime and at temperatures below 1000 K, line-center transmittances for absorption lines that are separated by less than about 0.5 cm^{-1} are subject to overlap error, because the widths of the lines are relatively large. This is evident from Eq. 7. At lower pressures and higher temperatures, however, the minimum line spacing requirements are greatly relaxed. Line overlap considerations are discussed further in later sections.

The transmittances of the absorption lines also depend on properties of the test environment: specifically, the path length, absorber concentration, temperature, and total pressure. If the test environment is such that one or both of the line-center transmittances is either very close to 100% or close to 0%, then the changes in transmittance with temperature will be small and of the same order as the measurement errors. Hence, the subsequent temperature measurement errors will be large. Although in most cases the properties of the test environment are fixed, the absorption line selection process does allow some control over transmittance values for a given environment. For example, two absorption lines whose STP linestrengths are as close as possible will yield significantly better measurement accuracy at low temperatures than that of two lines whose STP linestrengths differ by a relatively larger amount.

Carbon monoxide (CO) absorption lines were selected for this study, partly because of its abundance in most combustion processes where the dual-line ratio temperature-measuring technique might be useful. In addition, however, CO has some other attractive features. These are best described with the aid of Fig. 5, which shows an absorption spectrum of CO that was obtained with a Bomem model DA3.02 Fourier Transform Spectrometer and test cell. First, the separation between the fundamental lines (i.e., the 1-0 vibration lines) is approximately

$$\Delta\nu_{1\text{-}0} \approx 2B_e \approx 3.8 \text{ cm}^{-1},$$

where B_e is the rotational constant for CO (B_e = 1.931285). In most test situations, these lines are far enough apart to preclude significant overlap errors. Moreover, the fundamental vibration band and the 2-1 vibration band are intermeshed; hence, it is likely that there are a number of 1-0, 2-1 line pairs that meet the spacing requirements discussed previously. Although the 2-1 vibration lines cannot be resolved on Fig. 5, the band center position, which is at 2116.80 cm^{-1}, can be easily calculated from other CO molecular constants. Appendix B presents the equations that determine the spectrum of CO. These equations can be used to assess the suitability of other diatomic molecules provided that the molecular constants are known.

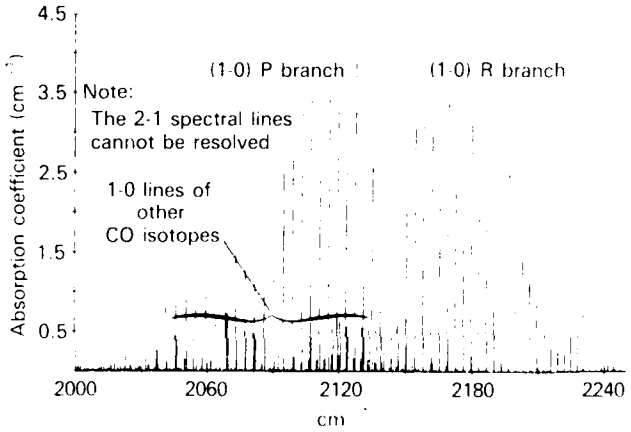

Figure 5 Absorption spectrum of CO measured using a Fourier transform spectrometer and test cell.

3.0 EXPERIMENTAL SETUP

The dual-line ratio technique was employed to measure gas temperatures in an absorption test cell. The primary goal was to evaluate the applicability of the technique, with particular emphasis toward measurements below 1000 K. The test setup and apparatus are described below.

3.1 TEST SETUP

Figure 6 shows the test setup. The diverging beam from the diode laser is collected and collimated by a 25 mm focal length (fl) BaF$_2$ lens. The collimated beam is chopped at 260 Hz and focused to the

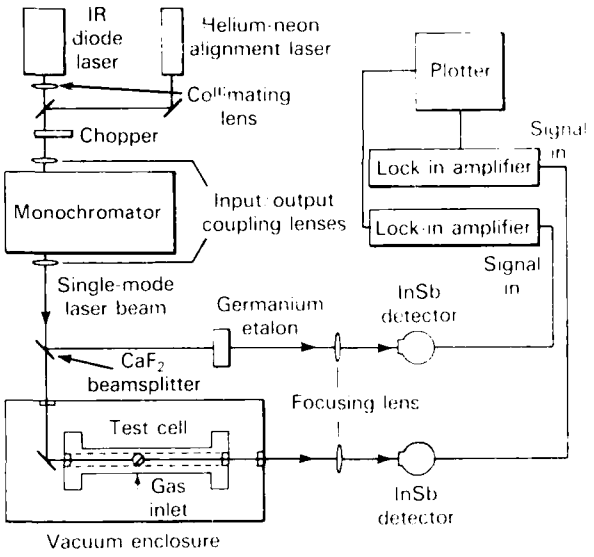

Figure 6 Experimental setup and apparatus.

monochromator input slit with a 37.5 mm fl BaF_2 lens. The 0.35 mm fl McPherson Model 270 monochromator serves as an optical bandpass filter to isolate a single laser mode. The monochromator wavelength dial coincides with the wavelength region of the absorption lines to be measured. The monochromator input-output slit width is 300 μm. This width is large enough to pass the single laser mode over the required tuning range, but small enough to ensure secondary mode rejection.

The monochromator output, which is subsequently recollimated by a second 37.5 mm fl BaF_2 lens, strikes a CaF_2 beamsplitter. The transmitted beam enters the vacuum enclosure through a BaF_2 window, reflects from a first-surface mirror through the test cell, and exits the vacuum enclosure through a second BaF_2 window. The heated test cell contains various mixtures of carbon monoxide (CO) and nitrogen (N_2). The beam reflected by the beamsplitter strikes a germanium Fabry-Perot etalon that has a free spectral range (FSR) of 0.0066 cm^{-1}. By counting etalon transmittance maxima, which occur when the laser wavelength is an integral multiple of twice the etalon optical thickness, the tuning rate of the laser can be monitored. The etalon was on loan from the Ohio State University, courtesy of R. Tolles.

The test cell and etalon outputs are each focused by a 200 mm fl BaF_2 lens to a liquid-nitrogen-cooled InSb detector. Two EG&G Lock-in Amplifiers, models 5206 and 5207, demodulate the detector outputs. A synchronization signal from the chopper supplies the lock-in amplifier reference signal. A [illegible] records the demodulated [illegible]

Proper alignment of the [illegible] is critical because, at best, the detected signal ratio is low owing to the low laser power (~1 mW) and the large attenuation through the components. The initial alignment is performed with a helium-neon (He-Ne) beam that is aligned coaxially with the diode laser beam. Fine adjustments are then made to lenses and mirrors to optimize the detected diode laser signal.

3.2 APPARATUS

The two components that are integral to this study are the diode laser system and the absorption test cell. Both components are described below.

3.2.1 The Diode Laser System

The diode laser system, manufactured by Spectra Physics, Laser Analytics Division, consists of the lasers and cold head, the cryogenic refrigerator, the vacion pump and control unit, the Model SP5720 cryogenic temperature stabilizer (CTS), and the model SP5820 laser control module (LCM).

The cold head, cryogenic refrigerator, vacion pump and the CTS form the closed-cycle cooling system that maintains the diode lasers at temperatures as low as about 13 K. Pressure lines circulate helium gas between the refrigerator and the cold head. The cold head compressor converts the helium gas to liquid. The liquid helium expands into a chamber and evaporates, cooling the cold finger where as many as four lasers are attached. The system is capsulated in a vacuum chamber to minimize heat transfer from the ambient surroundings. The vacion pump maintains the vacuum chamber below 1.0×10^{-5} torr. The laser temperature is set by adjusting a potentiometer on the CTS. The CTS regulates the temperature via sensors and a heating coil in the cold head.

The LCM controls the laser operating current. The controls include DC amplitude adjustment, slow sweep selection at three possible rates, and square, ramp, and sawtooth modulation up to 200 Hz. The LCM also contains safety features that prevent inadvertent overheating or overenergizing of the lasers.

The diode laser used in this study is of the lead-salt (PbSnTe) variety. The output power is about 1 mW. The laser typically operates simultaneously at 3 to 5 frequency modes. The linewidth of a single laser operating mode is specified by the manufacturer to about 1×10^{-4} cm^{-1}. It is this narrow linewidth, combined

with tuning capability, that makes diode lasers an excellent tool for high-resolution spectroscopy.

Coarse frequency tuning of the laser is performed by varying the temperature. Varying the laser temperature causes the laser modes to move discontinuously within about a 50 cm^{-1} range. Figure 7a characterizes the frequencies of the laser used for this study as a function of temperature. The optimum operating temperature of the laser is determined by setting the monochromator dial to the frequency of a candidate absorption line pair and incrementing the laser temperature until radiation is detected at the monochromator output. This process is iterated until a match is found between a laser frequency and an absorption line pair position. For these experiments, a laser temperature of 29 K was selected.

Continuous frequency tuning of the laser is performed by sweeping the power supply current. Figure 7b shows a series of monochromator scans that were each obtained at a different laser current at a laser temperature of 29 K. The figure demonstrates continuous tuning capability of a single laser mode over a 1.4 cm^{-1} range. This is verified by the quality of the etalon scan given in Fig. 7c.

3.2.2 The Test Cell

The absorption test cell was originally designed for spectroscopic studies of hot pressurized gases. Some design modifications were added in the course of this study to enhance the cell performance at higher temperatures.

Figure 8a illustrates the test cell. The cell, which is constructed of 316 stainless steel, is 12 in. long and has a center bore of 0.75 in. Optical access is provided by two sapphire windows, one at each end of the cell. Gas enters the cell through the vertical stem via a pneumatically-actuated normally-closed valve. The valve is activated by two solenoid valves and a 100 psi nitrogen supply. Pressure gauges connected to the lower stem in the right end-flange monitor the cell pressure. Although high pressures were not required for this study, the cell has been pressurized to 1000 psi in other experiments. The surface area of the cell between the end-flanges is instrumented with ceramic heating elements that are packed in ceramic insulation and radiation shielding. Two type-K thermocouples in contact with the outside wall at the center and end of the cell monitor the temperature.

Two major modifications were required to make the test cell suitable for these measurements. First, the window/end-cap assembly was redesigned to achieve higher temperatures. Second, a vacuum enclosure was constructed to capsulate the test cell and thereby improve

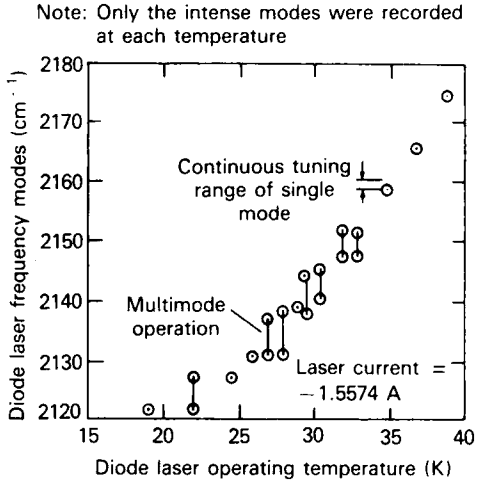

(a) Laser frequency versus operating temperature.

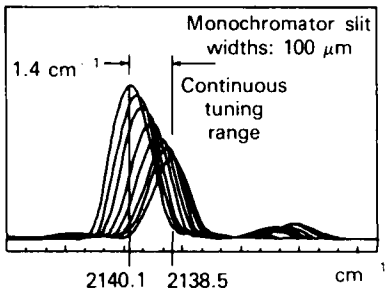

(b) Monochromator scans at different laser currents.

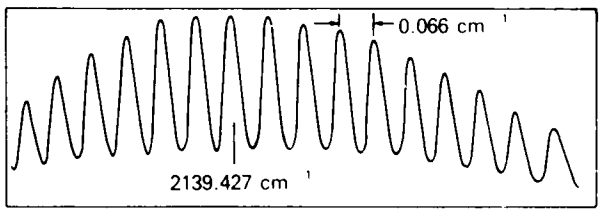

(c) Etalon transmittance as the laser current is scanned.

Figure 7 Diode laser tuning characteristics.

temperature uniformity along the cell length. These modifications are discussed below.

The original window assembly incorporated two 3-in.-dia., 0.25-in.-thick sapphire windows that were each sandwiched between an end-flange and end-cap and sealed with a silicon O-ring. Because the O-rings melt above 250°C, the assembly was replaced with modified end-caps each of which contained a 1-in.-dia., 0.25-in.-thick, sapphire window. Each window was specially brazed and sealed to the stainless steel by the California-based company, Ceradyne. Stainless steel O-rings were

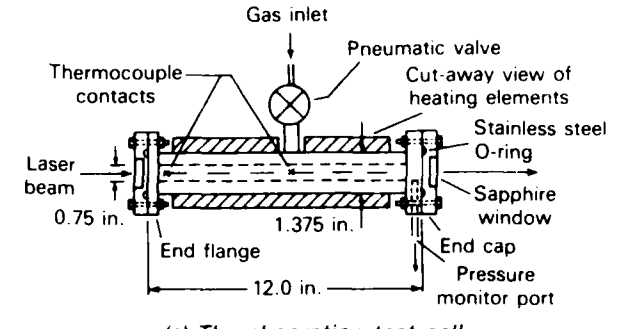

(a) The absorption test cell.

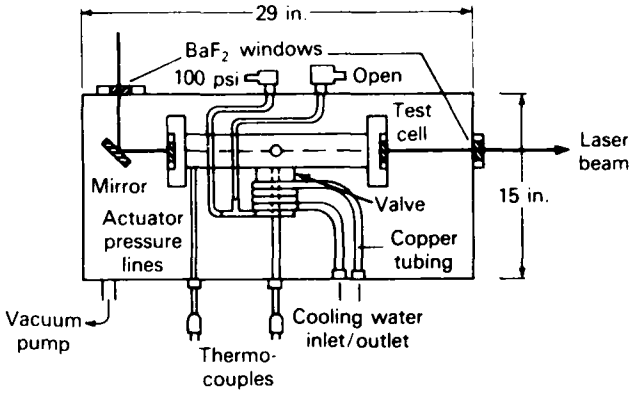

(b) Top view of inside the vacuum enclosure.

Figure 8 The test cell and vacuum enclosure configuration.

then used to seal the modified end-caps to the end-flanges. Initial experiments using these windows failed, however, because the windows fractured after a few temperature cycles of the test cell and had to be returned to Ceradyne for repair. The windows were eventually returned and successfully tested.

The temperatures between the center and end of the original version of the test cell differed by as much as 70°C. This temperature was unacceptable because experiments of the dual-line ratio technique require a reasonably homogeneous path. To improve temperature uniformity and to reduce heat loss, an aluminum vacuum enclosure was constructed to capsulate the test cell. Figure 8b shows the dimensions of the enclosure. During operation, the enclosure is evacuated to about 0.25 torr. Optical access for the laser beam is provided by two BaF_2 windows. Components in the vacuum enclosure are accessed from the top by removing two large plates and gaskets. The cell support platform is constructed of asbestos to minimize heat conduction to the enclosure. To preserve the seals in the pneumatically actuated valve, water-cooled copper tubing was wrapped around the valve piston housing.

The modification of the test cell window assembly and the construction of the vacuum enclosure increased the working temperature from about 250 to 500°C. Although there was some improvement in temperature uniformity across the cell, test results were still somewhat disappointing. The smallest temperature differential that could be achieved across the cell varied from about 20°C at lower temperatures to 35°C at higher temperatures. Clearly, the development of an absorption test cell with better temperature uniformity would be a primary goal of future studies.

4.0 MEASUREMENTS

Temperature measurements were conducted over a range from 385 to 840 K using two CO absorption line pairs that were selected from three absorption lines that were within the 1.4 cm^{-1} tuning range of the diode laser. One line pair consisted of

$C^{12}O^{16}$ 2-1 R(5) at 2138.911 cm^{-1}

and

$C^{12}O^{16}$ 1-0 P(1) at 2139.427 cm^{-1}

Temperature measurements using this pair were conducted in both the Doppler and collision regimes. The second line pair consisted of

$C^{12}O^{16}$ 2-1 R(5) at 2138.911 cm^{-1}

and

$C^{12}O^{18}$ 1-0 R(13) at 2139.914 cm^{-1} .

Two features of this line pair should be noted: first, the first absorption line is the same as that of the previous line pair, and second, the second line is of a different isotope than the first line. This combination was examined because the STP linestrengths of these lines differ only by an order of magnitude. The intent was to improve temperature sensitivity at lower temperatures. (For comparison, the STP linestrengths of the first line pair differ by about 10^4.) The use of the second line pair was limited, however, to pressures in the Doppler regime because at the higher pressures considered, the $C^{12}O^{18}$ line was completely overlapped by the stronger $C^{12}O^{16}$ fundamental line. To avoid confusion later, the first line pair of the same isotopes is called the matched line pair. The second line pair, of different isotopes, is called the mixed line pair.

This chapter describes the measurement procedures, the results, and the experimental errors.

4.1 MEASUREMENT PROCEDURES

Two parameters besides the absorption line profiles are required to measure the line-center transmittances of the absorption lines:

1. The background (i.e., the 100%) transmittance level at the respective line-centers, and
2. The baseline (i.e., the 0%) transmittance level at the respective line-centers.

As illustrated in Fig. 9, once these parameters and the absorption line profiles are known, the line-center transmittance is calculated from

$$T = \frac{\text{line minimum} - \text{baseline}}{\text{background} - \text{baseline}} .$$

Since the procedure to determine the background and baseline levels depended on the pressure regime, measurements in the two pressure regimes are described separately below.

Measurements in the collision regime were conducted using a mixture of CO and N_2 at a total pressure of 1 atm. Two laser frequency scans were performed for each temperature measurement. The first scan was performed with 1 atm of N_2 in the cell to record the background transmittance level. The test cell was evacuated and then both CO and N_2 were injected to a total pressure of 1 atm. The CO partial pressure was about 0.026 atm. The second scan was then performed to record the CO transmittance profiles. The baseline absorption level was obtained by blocking the diode laser beam. All three transmittance levels were recorded on the same plot. The data collection time for one temperature measurement was approximately 3 minutes.

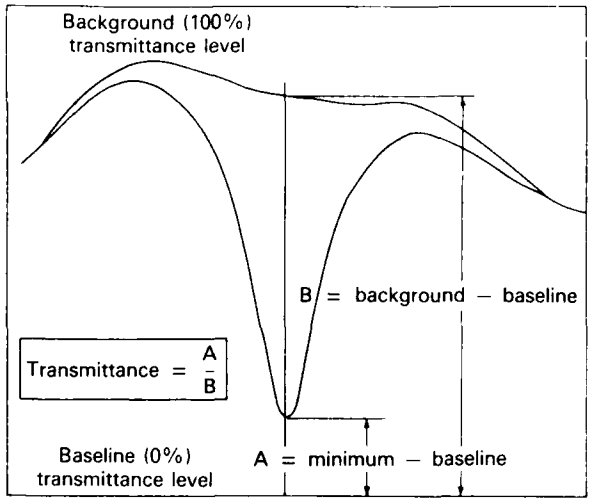

Figure 9 Absorption line transmittance measurement.

Measurements in the Doppler regime were conducted on CO alone, at pressures ranging from 0.0013 to 0.039 atm. Because of the narrow widths of the absorption lines, a separate background scan was not required. Rather, the background level at line-center was interpolated from points on the tails of the absorption lines. The baseline level was again determined by blocking the laser beam. For measurements of the mixed line pair, the baseline level was alternatively determined by injecting a large amount of CO into the test cell such that the line-center transmittance of the $C^{12}O^{16}$ fundamental line was 0%.

The tuning rate of the laser for each of the measurements described above was 7×10^{-3} cm^{-1}/s. This rate was selected to be slow enough to ensure adequate resolution of the transmittance profiles on the plotter, yet fast enough to ensure that test conditions would not change during the scan. The time constants of the lock-in amplifiers were set as long as possible (300 ms) to reject high frequency signal fluctuations.

The measured line-center transmittance values were inserted into either Eq. 15 or Eq. 16 to calculate the temperature.

4.2 RESULTS

The results are categorized according to the pressure regime in which the measurements were conducted.

4.2.1 Results of Measurements in the Doppler Regime

Figure 10 shows test results obtained with the mixed line pair at a CO pressure of 0.026 atm. The abscissa of the plot denotes the average thermocouple temperature. The extremes of the bars at each cell temperature point indicate the cell center-to-end temperatures. Note that the cell uniformity degrades with increasing temperature.

The temperature data points obtained with the dual-line ratio technique show an interesting trend. At lower temperatures, the technique predicts higher than the average thermocouple readings. Conversely, at higher temperatures, the technique predicts lower than the average thermocouple readings. The two coincide at 540 K.

The same measurements were repeated at a later date. In these tests, the time between successive temperature measurements were doubled to 90 minutes to guarantee that the temperature at the interior of the cell was stabilized. Figure 11 shows the results. The predicted temperature obtained from the mixed line pair shows the same trend as in Figure 10, except that in this case it is much better defined. The consistency between these measurements suggests that the actual averaged cell temperature is not equivalent to the average thermocouple readings. This is not unexpected since the temperature distribution across the cell varied with temperature.

Figure 11 also shows temperatures obtained with the matched line pair at a CO pressure of approximately 0.0013 atm. These measurements were performed in succession with the mixed pair measurements. Figure 12 shows one example of the transmittance profiles obtained for both line pairs. Except for one data point, the predicted temperature from the matched line pair is almost a constant factor lower than that predicted by the mixed line pair. This suggests a systematic error, perhaps due to an error in one of the AFGL parameters that was used to calculate the temperature.

To demonstrate the effect of such an error, the following assumptions were made:

1. The temperature predicted by the mixed line pair is correct,
2. The AFGL parameters for each absorption line of the mixed line pair is correct, and
3. The STP linestrength of the fundmental line of the matched pair ($C^{12}O^{16}$ 1-0 P(1)) is in error.

Using these assumptions, the value of the STP linestrength of $C^{12}O^{16}$ 1-0 P(1) line, which was required for the matched and mixed line pair predictions to be equal, was determined. The procedures and results are as follows.

First, using the temperature predicted by the mixed line pair, the CO pressure for the matched line pair mea-

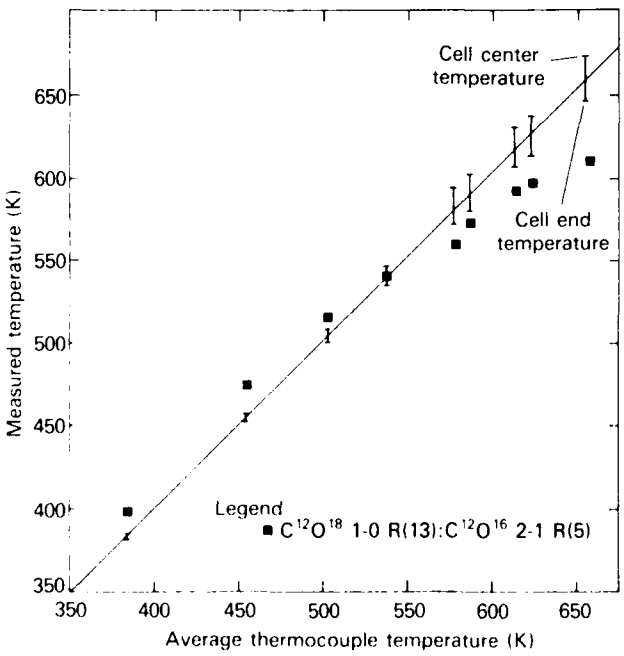

Figure 10 Temperature measurements in the Doppler regime.

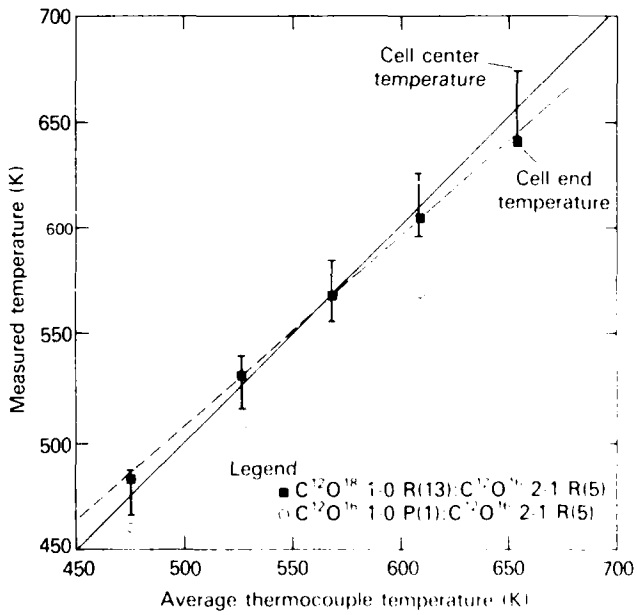

Figure 11 Temperature measurements in the Doppler pressure regime.

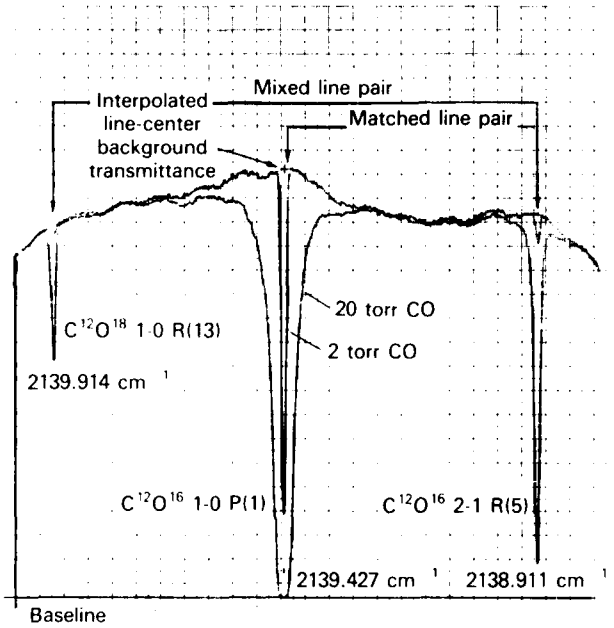

Figure 12 Transmittance profiles of three Doppler-broadened CO absorption lines.

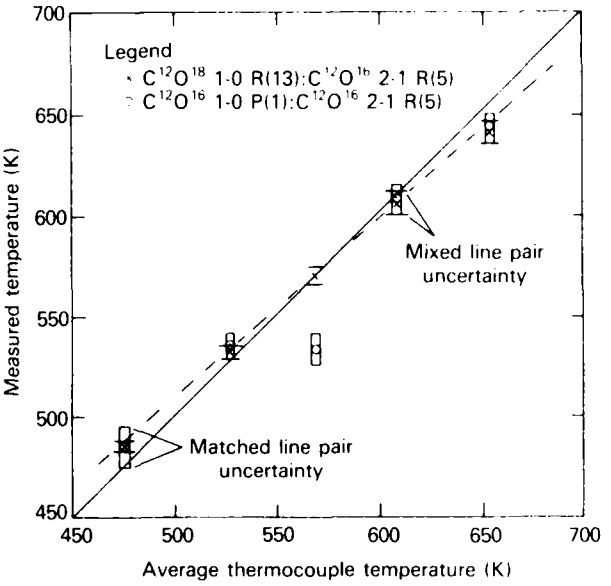

Figure 13 Temperature measurements in the Doppler pressure regime. (The modified STP line strength of $C^{12}O^{16}$ 1-0 P(1) was used.)

surement was calculated from the measured line-center transmittance and the AFGL parameters of the $C^{12}O^{16}$ 1-0 R(5) line. A calculation of the CO pressure was required because the pressure gauge used for the measurements was accurate to only ± 1 torr. Using the calculated pressure and the predicted mixed line-pair temperature, a value of the STP linestrength was calculated next, from the measured line-center transmittance value of the $C^{12}O^{16}$ 1-0 P(1) line. Equations 2, 4, 8, and 9 were used for the calculations. The calculations were performed at the two highest temperatures plotted on Fig. 11. The results give the values

$$S_0 = 1.225 \times 10^{-19} \text{ and } 1.283 \times 10^{-19} \text{ (mol./cm}^2\text{)} .$$

The value of the STP linestrength for the $C^{12}O^{16}$ 1-0 P(1) line on the AFGL listing is

$$S_0 = 0.893 \times 10^{-19} \text{ (mol./cm}^2\text{)} .$$

If the mean of the former values is used in the matched line temperature calculation, Fig. 13 shows that the matched and mixed line pair predictions match extremely well. The single erroneous data point is attributed to a noise spike that occurred at the transmittance minimum of one absorption line. The error bars at each data point will be discussed later.

The previous analysis provides some evidence that the STP linestrength value listed on the AFGL listing for the $C^{12}O^{16}$ 1-0 P(1) line might be in error. Intuitively, however, this seems unlikely, particularly for such an intense absorption line. Further study is required to resolve this issue. The goal of this exercise is to demonstrate that a systematic error, whatever the source, can explain the observed data.

4.2.2 Results of Measurements in the Collision Regime

Figure 14 shows temperature measurement results for a CO plus N_2 mixture at a total pressure of 1 atm as obtained for the matched line pair. Figure 15 shows a transmittance profile. For comparison, measurements were also made at the same cell temperatures using both the matched and mixed line pairs at Doppler pressures.

These data in Figs. 14 and 15 show a number of interesting features. First, the three matched line pair predictions obtained for each cell temperature are well grouped, regardless of the pressure regime over which the measurements were conducted. In addition, the matched line pair predictions are lower than the mixed line pair predictions, consistent with the results presented earlier. Most prominent, however, is that both predictions are higher than the thermocouple readings. This result was attributed to a fundamental flaw in the test setup, described next.

As shown in Fig. 8, the thermocouples are in point contact with the outer surface of the cell and restrained

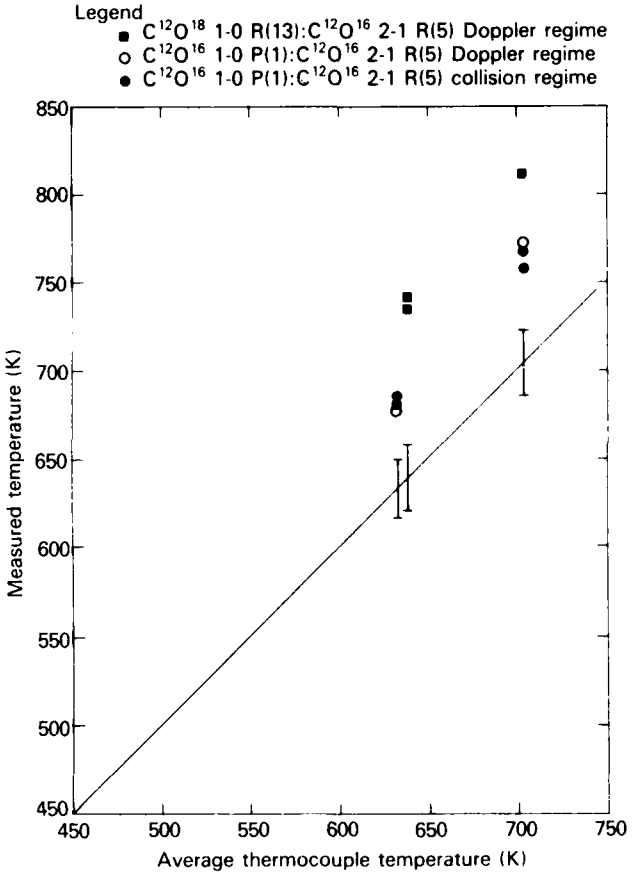

Figure 14 Temperature measurements in both the Doppler and collision regimes.

by fittings in the vacuum enclosure. A break in thermocouple contact with the cell by even 0.001 in. will result in significantly lower temperature readings. It is likely that such a break occurred in these measurements. Breaks in cell-to-thermocouple contact caused by thermal-expansion-induced movement of the test cell and vacuum enclosure have been observed in previous studies; however, this was the first occasion where apparently both thermocouples broke contact at the same time. For future measurement an alternative instrumentation technique is obviously required.

Figure 16 shows the upward shift of the matched line predictions if the modified STP linestrength that was calculated previously for the $C^{12}O^{16}$ 1-0 P(1) line is used in the temperature calculation. At the lower temperature the agreement between mixed and matched line pair predictions is excellent. The agreement at the higher temperature is also improved, although not quite as impressive.

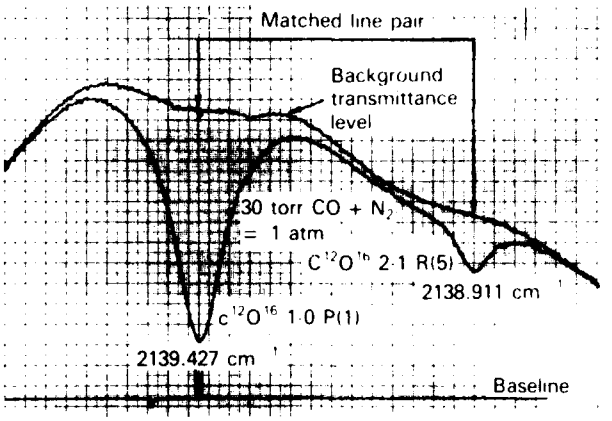

Figure 15 Transmittance profiles of two collision-broadened CO absorption lines.

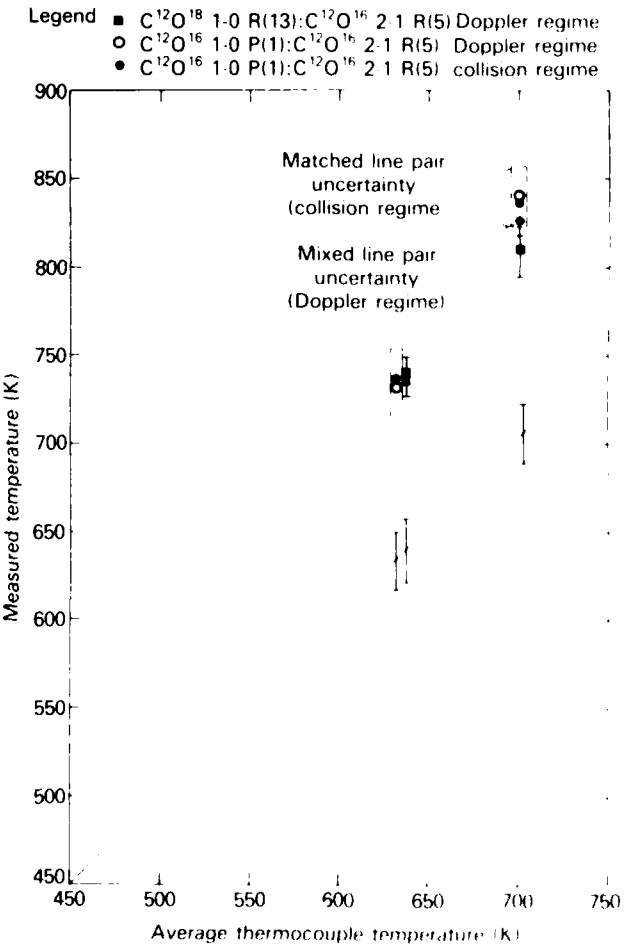

Figure 16 Temperature measurements in both Doppler and collision regimes. (The modified STP line strength of $C^{12}O^{16}$ 1-0 P(1) was used.)

4.3 ERROR ANALYSIS

The experimental errors that lead to transmittance measurement inaccuracies are discussed and quantified below. The results of this discussion are used to calculate the temperature measurement uncertainty of the dual-line ratio technique.

4.3.1 Transmittance Measurement Errors

Transmittance errors arise primarily from inaccuracies in identifying the line-center minimum of each absorption line profile and the line-center background transmittance levels. The accuracy to which these can be measured depends on the level of noise in the detection system, the stability of the test cell environment and diode laser beam, and the degree of absorption line overlap. The contribution of each of these factors depends on the properties of the test environment and the measurement procedure.

For measurements in the Doppler regime, the absorption linewidths are small enough and the line separations large enough to neglect potential line overlap errors. Moreover, since a measurement is made with a single transmittance profile (i.e., no separate background scan is required), the system stability between successive scans is not a factor. Therefore, the accuracy of measuring line-center transmittances of absorption lines in the Doppler regime depends primarily on the system noise and the capability of interpolating the background transmittance level from the tails of the absorption lines. Based on test experience, it is estimated that the transmittances of Doppler broadened lines can be measured to within approximately $\pm 0.5\%$.

For measurements at collision broadened pressures, however, absorption line overlap errors cannot be dismissed. Overlap error occurs when the tail of one absorption line overlaps the line-center frequency of the second absorption line. Figures 17 and 18, show transmittance profiles at various total pressures and temperatures that were calculated using Eqs. 2, 4, and 6. For the calculations, it was assumed that the line broadening characteristic of the CO, N_2 mixture was close enough to that of air to make the use of Eq. 7 (for the collision linewidth of an air-broadened absorption line) valid.

The figures indicate that absorption line overlap error will be most severe at lower temperatures and higher pressures. For example, calculations show that at 773 K and at a total pressure of 2 atm, line overlap will induce as high as a 2.5% error in the measured line-center transmittance of the $C^{12}O^{16}$ 2-1 R(5) line. However, the good agreement between matched line pair predictions obtained at Doppler and collision-broadened pressures, respectively, shown on Fig. 16, indicates that line overlap errors did not significantly affect the measurements at a total pressure of 1 atm.

Achieving acceptable stability between background and absorption line scans for the higher pressure measurements was a particular problem, primarily because of etalon-like effects from lenses and windows that were sensitive to even the smallest of system perturbations.

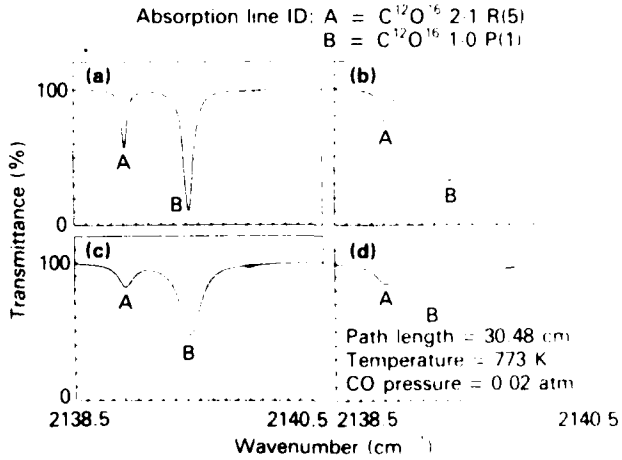

Figure 17 Theoretical transmittance profiles of two collision-broadened CO absorption lines at various pressures. Temperature = 773 K. (a) Total pressure = 0.5 atm; (b) Total pressure = 1.0 atm; (c) Total pressure = 1.5 atm; (d) Total pressure = 2.0 atm.

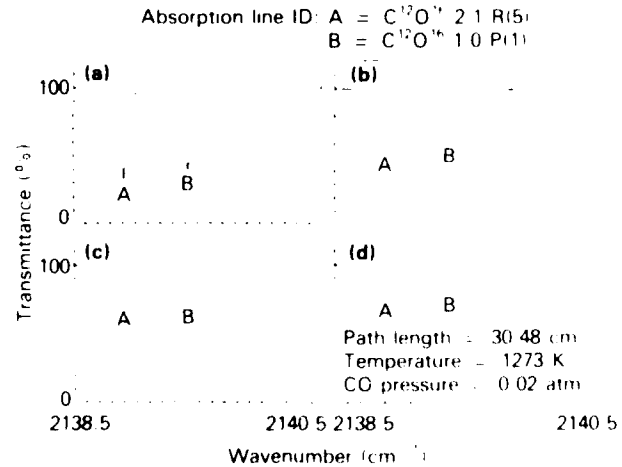

Figure 18 Theoretical transmittance profiles of two collision-broadened CO absorption lines at various pressures. Temperature = 1273 K. (a) Total pressure = 0.5 atm; (b) Total pressure = 1.0 atm; (c) Total pressure = 1.5 atm; (d) Total pressure = 2.0 atm.

Figure 19 illustrates an etalon effect that resulted from multiple reflections between the cell windows. Etalon effects are minimized by a combination of decollimating the laser beam and skewing the beam through the system elements such that multiple reflections do not overlap. Figure 20 demonstrates the scan-to-scan repeatability that was achieved in these measurements. The estimated transmittance measurement uncertainty is higher for collision-broadened lines than for Doppler-broadened lines because of the higher background uncertainty. Specifically, the estimated transmittance uncertainty is $\pm 1.0\%$.

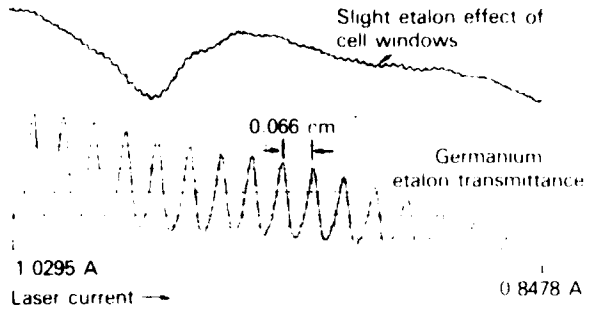

Figure 19 Etalon-like degradations in transmittance spectra.

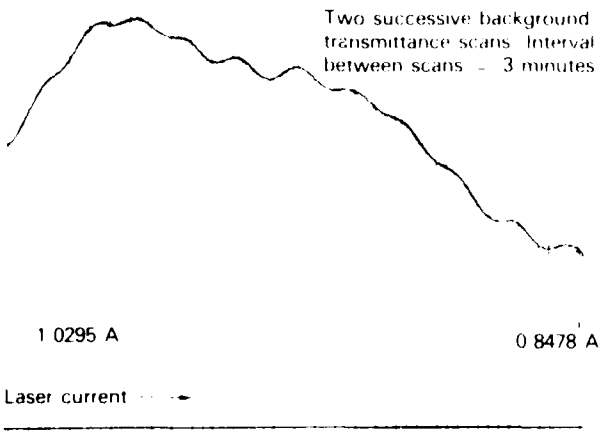

Figure 20 Scan-to-scan repeatability of the background transmittance level.

4.3.2 Temperature Uncertainty

The temperature error caused by the transmittance measurement error is derived by expanding the absorption coefficient ratio in a Taylor's series about a temperature T',

$$\frac{k_1}{k_2}(T') = \frac{k_1}{k_2}(T) + (T' - T)\left.\frac{d}{dT}\left(\frac{k_1}{k_2}\right)\right|_I + \ldots + .$$

Neglecting the higher order terms and solving for $(T' - T)$ gives

$$\Delta T \quad (T' \quad T) \cdot \frac{\frac{k_1}{k_2}(T') - \frac{k_1}{k_2}(T)}{\left.\frac{d}{dT}\left(\frac{k_1}{k_2}\right)\right|_I}$$

$$= \frac{\Delta\frac{k_1}{k_2}}{\left.\frac{d}{dT}\left(\frac{k_1}{k_2}\right)\right|_I} .$$

Differentiating either Eq. 14 or Eq. 15, depending on the pressure regime, gives $d/dT\,(k_1/k_2)_I$. Substituting this value above yields

$$\Delta T \quad \frac{\Delta\frac{k_1}{k_2}}{\frac{1.439\Delta E\, S_{01}\,\alpha_2}{T^2\, S_{02}\,\alpha_1}\exp\left[1.439\Delta E\left(\frac{1}{T_0} - \frac{1}{T}\right)\right]} \qquad (16)$$

Using Eq. 16, the temperature measurement uncertainty was calculated as follows.

The line-center transmittances of the two absorption lines were calculated from Eqs. 2, 4, 6, 7, 8, and 9. Figure 21a shows the result, as a function of temperature, for the matched line pair in the Doppler regime. Using the transmittance values, $k_1\ k_2$ was calculated from

$$\frac{k_1}{k_2} = \frac{ln(T_1 \pm \Delta\xi)}{ln(T_2 \pm \Delta\xi)} \qquad (17)$$

where $\Delta\xi$ is the transmittance measurement error that was estimated previously. Four curves of $k_1\ k_2$ were generated, one for each of the four combinations of Eq. 17. The envelope bounding the four curves defines the uncertainty in $k_1\ k_2$ caused by the transmittance

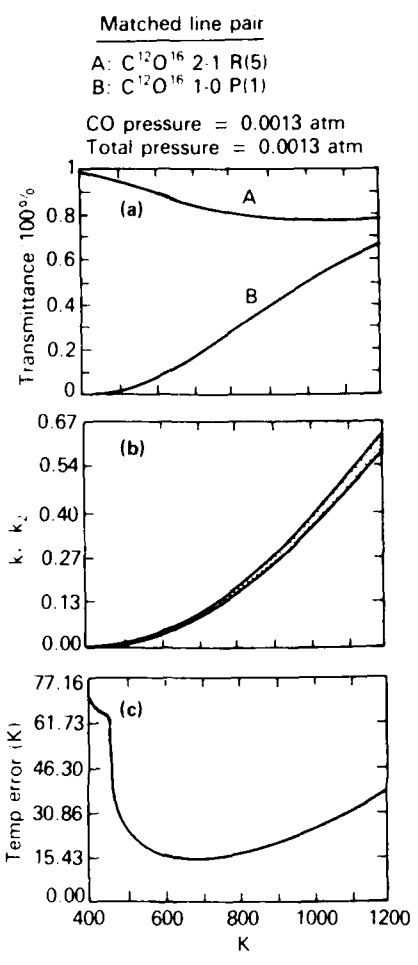

Figure 21

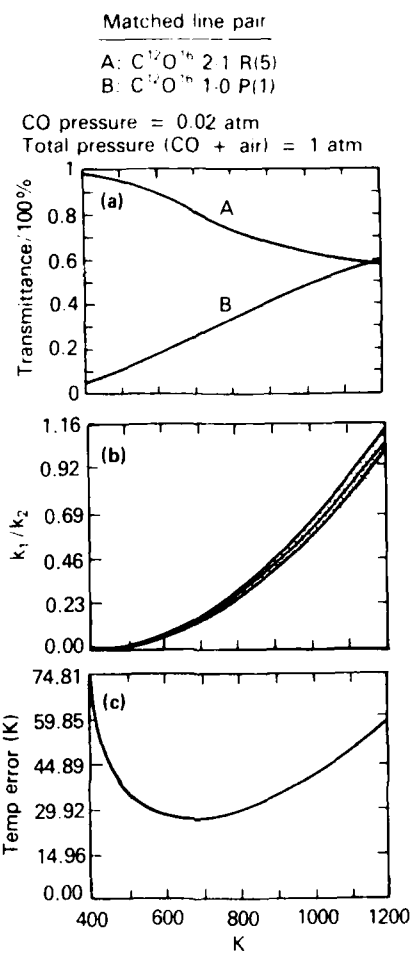

Figure 22

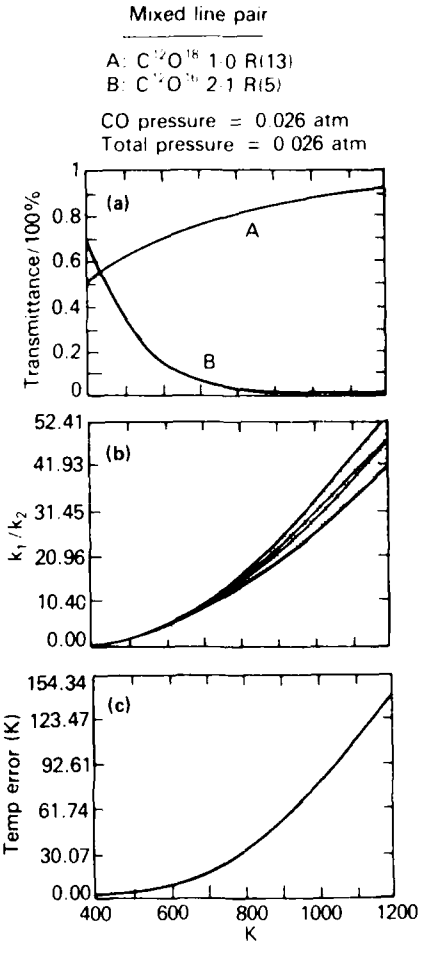

Figure 23

Figure 21 Temperature uncertainty calculations for the matched line pair in the Doppler-broadened regime. (a) The calculated line-center transmittances of the two absorption lines. (b) The uncertainty envelope of the absorption coefficient ratio as determined by applying a ±0.5% transmittance error to the transmittance values calculated above. (c) The temperature error caused by the uncertainty in the absorption coefficient ratio.

Figure 22 Temperature uncertainty calculations for the matched line pair in the collision-broadened regime. (a) The calculated line-center transmittances of the two absorption lines. (b) The uncertainty envelope of the absorption coefficient ratio as determined by applying a ±1% transmittance error to the transmittance values calculated above. (c) The temperature error caused by the uncertainty in the absorption coefficient ratio.

Figure 23 Temperature uncertainty calculations for the mixed line pair in the Doppler-broadened regime. (a) The calculated line-center transmittances of the two absorption lines. (b) The uncertainty envelope of the absorption coefficient ratio as determined by applying a ±0.5% transmittance error to the transmittance values calculated above. (c) The temperature error caused by the uncertainty in the absorption coefficient ratio.

measurement error. Figure 21b shows the k_1/k_2 uncertainty envelope for the matched line pair in the Doppler regime. From the previous section, the transmittance error is $\pm 0.5\%$. The size of the uncertainty envelope at each temperature was used for $\Delta k_1/k_2$ in Eq. 16. Figure 21c plots the corresponding temperature uncertainty as a function of temperature for the matched line pair in the Doppler regime. Figures 22 and 23 show similar plots for the matched line pair in the collision regime (for a transmittance error of $\pm 1\%$) and the mixed line pair in the Doppler regime (for a transmittance error of $\pm 0.5\%$), respectively.

The error bars on the data points of Figs. 12 and 16 are obtained from parts c of Figs. 21 through 23. The error bars indicate that the best accuracy at low temperatures and at pressures in the Doppler regime is achieved with the mixed line pair measurement. The temperature uncertainty is better than $\pm 1\%$. However, as temperature increases to about 800 K, the uncertainty increases to higher than $\pm 2\%$. At this temperature, the matched line pair (at pressures in the Doppler regime) gives better accuracy (i.e., about 1%), demonstrating the importance of the absorption line selection process in determining measurement accuracy in a given temperature range.

5.0 CONCLUSIONS

The results of this study demonstrate the use of the dual-line absorption ratio technique for measuring temperatures below 1000 K. For pressures in the Doppler regime the measurement uncertainty is estimated to be $\pm 1\%$ at 700 K. At the same temperature at a pressure in the collision regime, the uncertainty is approximately $\pm 2\%$. The use of absorption lines of different isotopes at pressures in the Doppler regime to improve low temperature measurement accuracy was also demonstrated. This work augments a previous study by Hanson et al.[6] that considered only temperatures above 1000 K, pressures in the collision regime, and absorption line pairs of the same isotope.

To calibrate the dual-line ratio technique accurately at temperatures below 1000 K, some improvements in the test apparatus are required. For example, a shorter path length test cell would provide significantly better temperature uniformity. In addition, an alternate technique of supporting the cell thermocouples is essential to prevent breaks in thermal contact with the test cell, caused by thermal expansion. Also, a pressure gauge that has a resolution of less than 1 torr would ensure a controlled cell environment for low pressure measurements. Lastly, replacing lenses in the optical system with off-axis aspheric mirrors and replacing plane parallel windows with wedged windows would greatly reduce etalon effects that degrade the transmittance spectra.

Since the precision of the STP absorption line parameters are crucial to the dual-line ratio technique, a calibration of the technique should include accurate measurement of these parameters. Because of its narrow single-mode linewidth, the tunable diode laser is an ideal tool for this. However, such measurements require a precisely controlled environment.

THE JOHNS HOPKINS UNIVERSITY
APPLIED PHYSICS LABORATORY
LAUREL, MARYLAND

APPENDIX A
The AFGL Absorption Line Compilation

The Air Force Geophysics Laboratory (AFGL) compilation lists absorption line parameters for the seven primary atmospheric species:

Molecule	Identification no. on AFGL listing
H_2O	1
CO_2	2
O_3	3
N_2O	4
CO	5
CH_4	6
O_2	7

The data for each absorption line includes ν_0, the line-center wavenumber, S_0, the linestrength (molecules/cm^2), α, the half-width (cm^{-1}/atm), E_l, the term value of the lower energy level (cm^{-1}), the transition quantum numbers, the date the data were acquired, the isotope, and the molecule identification number. An example of the AFGL listing is shown below.

A Fortran program that reads the AFGL 9-track magnetic tape is shown at the right. The program was developed on an IBM system 3033 computer.

```
/GEARATAB JOB (17413,,,N),'S.A. GEARHART',NOTIFY=GEAR,
/ USER=GEAR X6863
/*MAIN ORG=RM007
/ EXEC FHXLG
/F.SYSIN DD *
C*********************************************************************
C     THIS PROGRAM READS ABSORBTION LINE DATA FROM THE AFCRL DATA
C    TAPE(1984).  DATA IS PRINTED FOR A SPECIFIED WAVENUMBER RANGE.
C    EACH TAPE FILE CONTAINS DATA FOR A 100 WAVENUMBER RANGE.
C*********************************************************************
      DIMENSION GNU(40),S(40),ALPHA(40),EDP(40),TR1(40),TR2(40),TR3(40)
     1   ,TR4(40),TR5(40),TR6(40),TR7(40),TR8(40),TR9(40),I1(40),I2(40),
     2   I3(40)
      INTEGER*4 K
      READ (5,2)WAVE1,WAVE2
    2 FORMAT(2F10.0)
      WRITE(6,8)WAVE1,WAVE2
    8 FORMAT(1H1,20X,'AFGL ABSORBTION LINE PARAMETERS COMPILATION DATA'
     1 ,//,10X,'DATA FROM WAVENUMBER=',F10.3,'TO WAVENUMBER=',F10.3,
     2 //,'   WAVENO.  LINE STRNGH WIDTH  LOWER STATE       TRANSITION QU
     3ANTUM NUMBERS      DATE  ISOT  MOL',/)
      K=(ABS((WAVE1-1.0)/100))+10.0
    9 DO 50 I=1,500
        READ(K,15,END=60)ICARD
   15   FORMAT(I10)
        BACKSPACE K
        READ(K,20)(GNU(N),S(N),ALPHA(N),EDP(N),TR1(N),
     1  TR2(N),TR3(N),TR4(N),TR5(N),TR6(N),TR7(N),TR8(N),TR9(N),
     2  I1(N),I2(N),I3(N),N=1,ICARD)
   20   FORMAT(10X,40(F10.3,E10.3,F5.3,F10.3,8A4,A3,I3,I4,I3))
   30     DO 40 J=1,ICARD
            IF(GNU(J).LT.WAVE1)GO TO 40
            IF(I3(J).NE.5.) GO TO 40
            IF(GNU(J).GT.WAVE2)GO TO 100
C*********************************************************************
C         IF WRITE UNIT# IS 6, DATA GOES TO PRINTER                   *
C         IF WRITE UNIT# IS 8, DATA GOES TO DATA SET                  *
C*********************************************************************
            WRITE(6,35)GNU(J),S(J),ALPHA(J),EDP(J),TR1(J),TR2(J),
            WRITE(8,36)GNU(J),S(J),ALPHA(J),EDP(J),TR1(J),TR2(J),
     1      TR3(J),TR4(J),TR5(J),TR6(J),TR7(J),TR8(J),TR9(J),I1(J),
     2      I2(J),I3(J)
   35       FORMAT(F10.3,2X,E10.3,2X,F5.3,2X,F10.3,2X,8A4,A3,2X,I3,
     1      2X,I4,2X,I3)
   36       FORMAT(F10.3,E10.3,F5.3,F10.3,8A4,A3,I3,I4,I3)
   40     CONTINUE
        IF(ICARD.NE.40.)GO TO 60
   50 CONTINUE
   60 REWIND K
      K=K+1
      GO TO 9
  100 STOP
      END
/G.FT08F001 DD DSN=FIC.WJT.SHARE.AFGL,
/ DISP=(NEW,CATLG,DELETE),UNIT=SAVE,
/ DCB=(LRECL=80,BLKSIZE=6160,RECFM=FB),
```

WAVENO.	LINE STRNGH	WIDTH	LOWER STATE	TRANSITION QUANTUM NUMBERS	DATE	ISOT	MOL
2139.174	0.997E-23	0.100	307.916	10 8 2 11 9 3 2 0 0 0 0 0	79	666	3
2139.203	0.324E-22	0.064	2470.631	0 2 2 1 0 2 2 0 P 55C	13	446	4
2139.216	0.169E-22	0.073	2562.227	0 3 3 1 0 3 3 0 P 43D	13	446	4
2139.217	0.169E-22	0.073	2562.227	0 3 3 1 0 3 3 0 P 43C	13	446	4
2139.238	0.119E-21	0.077	892.236	0 1 1 1 0 1 1 0 P 27C	13	456	4
2139.241	0.179E-24	0.068	1748.578	2 1 1 0 1 0 2 2 0 1 P 32	482	626	2
2139.271	0.325E-22	0.064	2470.033	0 2 2 1 0 2 2 0 P 55D	13	446	4
2139.278	0.101E-24	0.066	2318.541	7 3 5 7 2 6 1 0 0 0 1 0	180	161	1
2139.317	0.914E-26	0.066	1945.796	1 3 3 0 1 0 2 2 0 1 R 39	482	626	2
2139.328	0.272E-25	0.067	2597.898	1 1 1 1 2 1 1 1 0 1 P 36	482	626	2
2139.329	0.794E-22	0.045	1631.384	10 7 4 9 6 3 0 1 0 0 0 0	180	161	1
2139.333	0.341E-22	0.100	529.577	30 5 25 31 6 26 2 0 0 0 0 0	79	666	3
2139.348	0.382E-22	0.055	2510.107	0 0 0 1 0 0 0 0 P 77	13	446	4

APPENDIX B
The Spectra of Diatomic Molecules

The equations that determine the spectra of diatomic molecules are discussed briefly below. A more complete development can be found in Ref. 8.

Solution of the Schrödinger equation for a vibrating-rotator gives the values of the quantized energy values of a diatomic molecule:

$$E = G(V)hc + F_V(J)hc \ , \qquad \text{(B-1)}$$

where V and J are the respective vibration and rotational quantum numbers. The first term of Eq. B-1, representing the energy of an anharmonic oscillator, is given by

$$G(V)hc = (\omega_0 V - \omega_0 x_0 V^2 + \omega_0 y_0 V^3 + \ldots)hc \ , \qquad \text{(B-2)}$$

where

$$\begin{aligned} \omega_0 &= \omega_e - \omega_e x_e + 3\omega_e y_e/4 + \ldots , \\ \omega_0 x_0 &= \omega_e x_e - 3\omega_e y_e/2 + \ldots , \\ \omega_0 y_0 &= \omega_e y_e + \ldots . \end{aligned} \qquad \text{(B-3)}$$

The first term of Eq. B-2 represents the energy of a simple harmonic oscillator. The other terms in the series are required in order to obtain the energy of an anharmonic oscillator, such as is observed in nature. (The harmonic oscillator has energy levels of equal spacing—the anharmonic oscillator has energy levels that become closer as V increases.) The second term in Eq. B-1 represents the energy of a nonrigid rotator, given by

$$F(J)hc = [B_e J(J+1) - D_e J^2 (J+1)^2]hc \ . \qquad \text{(B-4)}$$

The first term in Eq. B-4 contains the rotational constant B_e, which is inversely proportional to the molecular moment of inertia. The second term, which is small for small J, accounts for the change in the moment of inertia caused by centrifugal stretching of the molecule. Note that Eq. B-4 neglects the effect of vibration on the moment of inertia since this is small for small values of V. The molecular constants, ω_e, $\omega_e x_e$, $\omega_e y_e$, B_e, and D_e, in Eqs. B-2 and B-4 are tabulated in Ref. 8 for a number of diatomic molecules. Using these constants, the energy levels can be determined, as depicted in Fig. B-1a.

Using Eqs. B-1 to B-4 and the quantum-mechanical selection rules for a diatomic molecule, which dictate that energy transitions only occur in such a way that both V and J change by ± 1, respectively, the frequencies of the spectral lines can be determined. A change in J of 1 denotes an R transition; a change in J of -1 denotes a P transition, as indicated in Fig. B-1b. Thus, for a given vibration transition, there is a host of narrowly spaced spectral lines corresponding to the changes in rotational energy. These lines are centered about the frequency (in wavenumbers)

$$\nu_0 = G(V'') - G(V') \qquad \text{(B-5)}$$

where V' and V'' are the initial and final quantum numbers, respectively. Using Eqs. B-4 and B-5, the frequencies of the spectral lines are, therefore, given by

$$\nu_R = \nu_0 + F(J+1) - F(J)$$

for the R transitions, and

$$\nu_P = \nu_0 + F(J-1) - F(J)$$

for the P transitions. Neglecting the centrifugal force term in Eq. B-4, these equations reduce to

$$\nu_R = \nu_0 + 2B_e + 2B_e J \qquad \text{(B-6)}$$

$$\nu_P = \nu_0 - 2B_e J \qquad \text{(B-7)}$$

The rotation-vibration of HCl for the $V = 0$ to $V = 1$ transition (called the fundamental) is shown in Fig. B-1c. Note that the R branch is on the higher frequency side of ν_0. In addition, there is no absorption line at ν_0 because the selection rules preclude a $J = 0$ transition. The spacing between fundamental lines is approximately

$$\nu_{R+1} - \nu_R \approx 2B_e \ . \qquad \text{(B-8)}$$

[8] G. Herzberg, *Molecular Spectra and Molecular Structure: I. Spectra of Diatomic Molecules*, 2nd ed., Van Nostrand Reinhold Co., New York (1950).

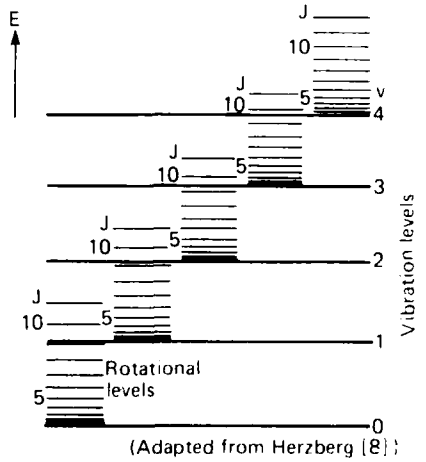

(a) Energy levels of a vibrating-rotator.

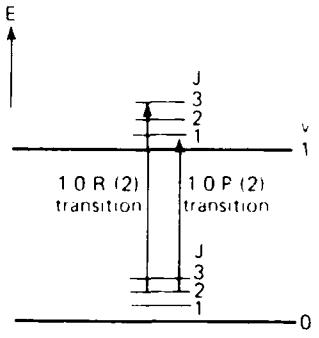

(b) R and P energy transitions.

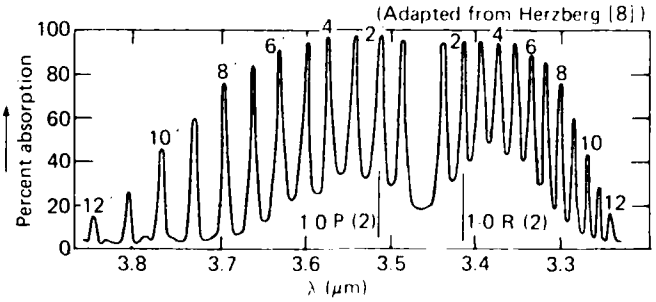

(c) Vibration-rotation spectrum for the fundamental transitions (v = 0 → 1) of HCl.

Figure B-1 Energy levels and spectrum of a diatomic molecule.

REFERENCES

[1] J. Reid, J. Shewchun, B. K. Garside, and E. A. Ballik, "Detecting Pollutants in the Atmosphere," *Appl. Opt.* **17** (Jan 1978).

[2] D. T. Cassidy and J. Reid, "Atmospheric Monitoring of Trace Gases," *Appl. Opt.* **21** (Apr 1982).

[3] M. D. Levenson, "Coherent Raman Spectroscopy," *Phys. Today* (May 1977).

[4] L. E. Lee, R. Turner, and R. C. Benson, "Optical Measurements for Ramjet Engine Development," *Johns Hopkins APL Tech. Dig.* (Jul - Sep 1983).

[5] J. Y. Wang, "Laser Absorption Methods for Simultaneous Determination of Temperature and Species Concentration Through a Cross Section of Radiating Flow," *Appl. Opt.* **15** (Mar 1976).

[6] R. K. Hanson and P. K. Falcone, "Temperature Measurement Technique for High-Temperature Gases Using a Tunable Diode Laser," *Appl. Opt.* **17** (Aug 1978).

[7] R. A. McClatchey, *AFCRL Atmospheric Absorption Line Parameters Compilation*, distributed by National Technical Information Service (Jan 1973).

[8] G. Herzberg, *Molecular Spectra and Molecular Structure: I. Spectra of Diatomic Molecules*, 2nd ed., Van Nostrand Reinhold Co., New York (1950).

INITIAL DISTRIBUTION EXTERNAL TO THE APPLIED PHYSICS LABORATORY*

The work reported in TG 1365 was done under Navy Contract N00039-87-C-5301 and is related to Task X8G5, supported by The Johns Hopkins University/Applied Physics Laboratory Independent Research and Development Program.

ORGANIZATION	LOCATION	ATTENTION	No. of Copies
DEPARTMENT OF DEFENSE			
Secretary of Defense	Washington, DC 20301	G. C. Kopesak, OUSDRE (ET)	1
Defense Technical Information Center	Alexandria, VA 22314	Accessions	12
DEPARTMENT OF THE NAVY			
CNO	Washington, DC 20350	OP 98	1
		OP 983	1
		OP 987	1
		OP 987B	2
		OP 35	1
		OP 351	1
		OP 352	1
		OP 3521	1
		OP 355	1
		OP 355W	1
		OP 507D	1
Office of the Assistant Secretary of the Navy (RE&S)	Washington, DC 20350	Edward Donalson	1
		Charles Kincaid	1
		J. R. Whalen	1
		R. J. Rumpf	1
		Ann Berman	1
		J. A. Jacobs	1
NAVSEASYSCOM	Washington, DC 22202	SEA 06	1
		SEA 06A	1
		SEA 06A1	1
		SEA 06AX	1
		SEA 06P	1
		SEA 06R	1
		SEA 62	1
		SEA 62B	1
		SEA 62D	2
		SEA 62D1	2
		SEA 62D2	2
		SEA 62D22	1
		SEA 62D3	1
		SEA 62D4	1
		SEA 62D52	1
		SEA 62Z	1
		SEA 62Z1	1
		SEA 62Z2	1
		SEA 62Z3	1
		SEA 62Z3B	1
		SEA 62Z31	2
		SEA 62Z31B	1
		Lib., SEA 9961	2
		PMS 400	1
		PMS 400B	1
NAVAIRSYSCOM	Washington, DC 22202	AIR 320	1
		AIR 320B	1
		AIR 320D	1
		AIR 320R	1
		AIR 06	1
		AIR 0623	1
		Lib., AIR 7226	2
NAVPRO	Laurel, MD 20707		1
Naval Surface Weapons Center	Dahlgren, VA 22448	NSWC DL D2W	1
		NSWC DL G06	1
		NSWC DL G21	1
		NSWC DL G22	1
		NSWC DL G24	1
		Library	2
	White Oak, MD 20903-5000	NSWC WO G40	1
		NSWC WO K22	1
		NSWC WO N12	1
		Library	2

Requests for copies of this report from DoD activities and contractors should be directed to DTIC, Cameron Station, Alexandria, Virginia 22304-6145 using DTIC Form 1 and, if necessary, DTIC Form 55.

*Initial distribution of this document within the Applied Physics Laboratory has been made in accordance with a list on file in the APL Technical Publications Group

INITIAL DISTRIBUTION EXTERNAL TO THE APPLIED PHYSICS LABORATORY*

ORGANIZATION	LOCATION	ATTENTION	No. of Copies
Naval Wespons Center	China Lake, CA 93555-6001	3906	2
		3921	1
		3941	1
		3942	1
		3854	1
		Library	1
Office of Naval Technology	Arlington, VA 22209	ONT 07C	1
		ONT 0712	1
		ONT 0713	1
Pacific Missile Test Center	Pt. Mugu, CA 93042	4045	1
U.S. Naval Academy	Annapolis, MD 21402	Dir. Research	2
DEPARTMENT OF THE ARMY			
Missile Command	Redstone Arsenal, Huntsville, AL 35898	DRSMI OD	1
		DRSMI RR	1
Ballistic Missile Defense Advanced Technology Center	Huntsville, AL 35807	ATC 0	1
		Gene Tidwell, SDC HEDI	1
		Claud F. Martin, DASD H 4B	1
		Tony Street, DASD H WK	1
		Price Boyd, DASD H WK	1
DEPARTMENT OF THE AIR FORCE			
Air Force Armament Division	Eglin AFB, FL 32542	AD XRG	1
Aeronautical Systems Division	Wright Patterson AFB, Dayton, OH 45433	YYM	1
CONTRACTORS			
Acurex Corporation	Huntsville, AL 35806	F. Strobel	1
Aerojet Electro Systems Co.	Azusa, CA 91702	Irwin Weiss	1
Coors Porcelain Co.	Golden, CO 80401	D. Roy	1
General Dynamics	Pomona, CA 91766	H. J. Meltzer	2
		R. M. Pietrasz	1
		R. Parker	1
		I. Stamper	1
GTE Laboratories, Inc	Waltham, MA 02254	W. H. Rhodes	1
Hughes Aircraft Co.	Canoga Park, CA 91304	R. R. Miller	2
		A. V. Funari	1
		Dennis Quan	1
		R. L. Sendall	1
		Richard Murray	1
Martin Marietta Corp	Orlando, FL 32805	John Sura	2
		A. F. Davidoff	1
McDonnell Douglas Aircraft Co.	St. Louis, MO 63166	T. F. Reilly	2
MIT Lincoln Laboratories	Lexington, MA 02173	L. B. Anderson	1
Raytheon Corporation	Bedford, MA 01730	A. F. Franz	2
Raytheon Corporation Research Div	Lexington, MA 02173	R. L. Gentilman	1
UNIVERSITIES			
Ohio State University	Columbus, OH 43210	R. K. Long	1

END

DATE

FILMED

FEB.

1988